UC Davis

UC Davis Previously Published Works

Title

Evolution of spatial resolution in breast CT at UC Davis

Permalink

https://escholarship.org/uc/item/46g4m9zd

Journal

Medical Physics, 42(4)

ISSN

0094-2405

Authors

Gazi, Peymon M

Yang, Kai

Burkett, George W

et al.

Publication Date

2015-04-01

DOI

10.1118/1.4915079

Peer reviewed

eScholarship.org Powered by the California Digital Library
University of California

Evolution of spatial resolution in breast CT at UC Davis

Peymon M. Gazi
Department of Biomedical Engineering, University of California, Davis, One Shields Avenue, Davis, California 95616

Kai Yang
Department of Radiological Sciences, University of Oklahoma Health Sciences Center, 940 N.E. 13th Street, Nicholson Tower, Oklahoma City, Oklahoma 73104

George W. Burkett, Jr. and Shadi Aminololama-Shakeri
Department of Radiology, University of California, Davis Medical Center, 4860 Y Street, Suite 3100 Ellison Building, Sacramento, California 95817

J. Anthony Seibert and John M. Boone[a)]
Department of Biomedical Engineering, University of California, Davis, One Shields Avenue, Davis, California 95616 and Department of Radiology, University of California, Davis Medical Center, 4860 Y Street, Suite 3100 Ellison Building, Sacramento, California 95817

(Received 5 August 2014; revised 9 February 2015; accepted for publication 22 February 2015; published 27 March 2015)

Purpose: Dedicated breast computed tomography (bCT) technology for the purpose of breast cancer screening has been a focus of research at UC Davis since the late 1990s. Previous studies have shown that improvement in spatial resolution characteristics of this modality correlates with greater microcalcification detection, a factor considered a potential limitation of bCT. The aim of this study is to improve spatial resolution as characterized by the modulation transfer function (MTF) via changes in the scanner hardware components and operational schema.
Methods: Four prototypes of pendant-geometry, cone-beam breast CT scanners were designed and developed spanning three generations of design evolution. To improve the system MTF in each bCT generation, modifications were made to the imaging components (x-ray tube and flat-panel detector), system geometry (source-to-isocenter and detector distance), and image acquisition parameters (technique factors, number of projections, system synchronization scheme, and gantry rotational speed).
Results: Characterization of different generations of bCT systems shows these modifications resulted in a 188% improvement of the limiting MTF properties from the first to second generation and an additional 110% from the second to third. The intrinsic resolution degradation in the azimuthal direction observed in the first generation was corrected by changing the acquisition from continuous to pulsed x-ray acquisition. Utilizing a high resolution detector in the third generation, along with modifications made in system geometry and scan protocol, resulted in a 125% improvement in limiting resolution. An additional 39% improvement was obtained by changing the detector binning mode from 2×2 to 1×1.
Conclusions: These results underscore the advancement in spatial resolution characteristics of breast CT technology. The combined use of a pulsed x-ray system, higher resolution flat-panel detector and changing the scanner geometry and image acquisition logic resulted in a significant fourfold improvement in MTF. © *2015 American Association of Physicists in Medicine.* [http://dx.doi.org/10.1118/1.4915079]

Key words: breast imaging, computed tomography, cone-beam CT, modulation transfer function

1. INTRODUCTION

The utility of breast cancer screening using digital mammography has come under criticism in recent years,[1,2] despite the significant reduction in breast cancer mortality that has occurred in the United States and other countries when mammographic screening programs were introduced. Nevertheless, many researchers have studied alternate technologies for breast imaging, some in the context of breast cancer screening and others specifically developed to be used during the diagnostic exam for breast cancer.

Mammography has several shortcomings. One of these is its decreased sensitivity in breasts with predominantly dense parenchyma.[3] This is partly a result of the depiction of the three-dimensional (3D) breast in a two-dimensional (2D) format. Tissue overlap contributes to the masking of occult cancers and the creation of fictitious lesions by superimposition of adjacent normal tissues. Efforts to overcome these shortcomings of routine mammography have led to the development of newer breast imaging modalities, such as dynamic contrast enhanced magnetic resonance imaging (MRI), digital breast tomosynthesis (DBT), whole

breast ultrasound (WBUS), and dedicated breast computed tomography (bCT).

Currently, MRI is most commonly used in women at high risk of developing breast cancer as a screening supplement to mammography.[4] Other common indications for MRI are evaluation of extent of disease and neoadjuvant chemotherapy treatment monitoring for locally advanced breast cancer. Lack of ionizing radiation and high sensitivity when combined with mammography is some of the advantages of MRI. However, lower specificity, requirement of intravenous contrast, high cost, lower patient tolerance, and lack of access have prevented this technique from replacing routine mammograms.

Targeted ultrasound is routinely used as an adjunct to mammography for problem solving and biopsy planning. The advantages of ultrasound are wide availability, lack of ionizing radiation, and relatively low cost when compared to other techniques such as breast MRI. More recently, ultrasound has been studied as a supplemental screening tool.[5] The largest of these trials[6] showed an increased cancer yield when whole breast ultrasound was added to screening mammography. However, this gain was balanced with lower specificity and positive predictive value. Moreover, the exams performed by physicians were laborious and time consuming.

A modified mammographic technique, DBT attempts to overcome some of the challenges posed by tissue superimposition. A series of low dose images are produced through the compressed breast and reconstructed into a volumetric 3D dataset. Reconstructed images are then viewed individually or as a cine-loop.[7] DBT is a FDA approved modality for both screening and diagnosis[8] and has tomographic properties.[9] However, due to the limited angular acquisition, it is not considered to be a true 3D imaging modality.[10]

Computed tomography of the breast is a true 3D imaging modality and therefore delivers coherent views in three orthogonal views, as well as off-axis multiplanar views. One of the most important issues facing the development of bCT, especially in light of the exceedingly high spatial resolution of digital mammography, is to deliver high spatial resolution while also delivering the excellent contrast resolution that computed tomography is known for. Our laboratory at UC Davis has developed four different dedicated breast CT systems, spanning essentially three generations of design evolution. In this communication, we chronicle the spatial resolution characteristics of these three dedicated bCT generations.

2. METHODS AND MATERIALS

2.A. System setup

Following the same design as previously reported,[11–13] a pendant-geometry, cone-beam breast CT scanner was designed and fabricated in our laboratory.[14] An exterior view of the system is shown in Fig. 1.

2.A.1. Hardware

The gantry design includes a pulsed x-ray tube (M-1500, Varian Medical Systems, Salt Lake City, UT), a flat-panel detector (DEXELA 2923MAM, Perkin Elmer, Santa Clara, CA),

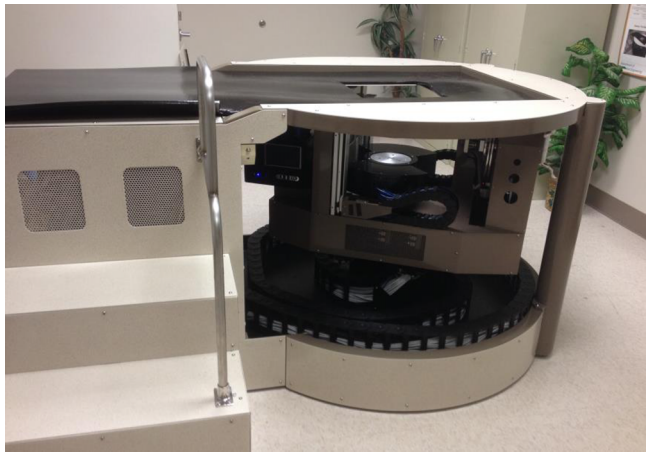

FIG. 1. Photograph of the latest UC Davis prototype of dedicated breast CT.

and a custom-designed filter and collimator changer assembly that provides six filter and six collimator options for specific scan procedures. Three vertical ball drives enable the translation along the axis perpendicular to the gantry rotation plane, one for the x-ray tube assembly and two for the embedded dedicated breast positron emission tomography (PET) scanner heads. The flat-panel detector, specifically designed for full-field breast imaging applications, features a 0.45 mm thick thallium-activated structured cesium iodide (CsI:Tl) scintillator coupled to complementary metal oxide semiconductor (CMOS) active detector elements (dexel) sensors, attached to 14 bit analog to digital converters. Each dexel contains an option for switching between two modes: low full well (LFW) and high full well (HFW). The LFW mode features lower read noise at the expense of reduced full well capacity. The x-ray detector was set to work in LFW mode during all the experiments reported in this paper. The detector provides an active field of view of 29×23 cm^2 with a small upper bezel (~3 mm) which translates into greater chest wall coverage than previous generation breast CT systems. The dexel pitch at native binning mode is 75×75 μm with a typical fill factor of 84%.[15]

The x-ray source, specifically designed for breast scanning purposes, is a water-cooled, rotating anode x-ray tube with a nominal focal spot size of 0.3 mm coupled with a 14 kW rad/pulse-rad x-ray generator (CMP200SE, CPI, Ontario, Canada). The x-ray focal spot distribution was measured with a 0.030 mm pinhole camera made from a 90:10 gold-platinum alloy (07-613, Nuclear Associates, Carle Place, NY). A phantom was placed near the x-ray tube's housing (distance between the pinhole and focal spot was 78 mm), resulting in a magnification factor of 8.8:1. The phantom was positioned to align the pinhole with the central ray, resulting in the projection of the focal spot on the previously calculated incident point of the central ray on the flat-panel detector. A 0.25 mm layer of additional copper filter was used to protect the dexels from saturation. A dexel binning mode of 2×2 was used for the detector, producing an effective dexel size of 0.150 mm. Three hundred images were acquired during each experiment, which were flat-fielded and averaged to reduce noise.

The gantry is mounted onto an integrated bearing-motor-encoder system with nominal peak continuous torque of

600 Nm with 1 048 576 pulses per revolution encoder resolution (SGMCS Direct Drive Servo Motor, Yaskawa, Japan). A computer was physically positioned on the gantry behind the detector to capture and store the high bandwidth stream of projection images from the detector and to control the gantry-mounted motors and sensors. An external computer at the system console handles synchronization and control of other scanner components. Figure 2 illustrates the gantry design and components.

2.A.2. Synchronization

Initiating an acquisition cycle, the control computer issues a command to the microcontroller board, which sends a pulse to the x-ray detector. The detector's feedback signal is then sent to the x-ray generator. An x-ray exposure is initiated, triggering a feedback signal to the gantry motor controller. Upon receipt of the signal, the angular position of the gantry motor is sent to the control computer. This completes the feedback loop for each acquired projection image. All feedback signals are denoised using RC circuits to remove the short jitter variations that impact the synchrony of the CT imaging chain.

2.A.3. Geometry

In order to achieve the same breast coverage as the previous generations of UC Davis breast CT systems[16] when accounting for the smaller flat-panel detector, the magnification factor in scanner Doheny was reduced from 1.9 to 1.4. Geometric calibration of the system[17] shows a source-to-detector and source-to-isocenter distance of 69.9 and 50.2 cm, respectively. The cone angle for the prototype ranges from −3.2° at the top to 15.8° at the bottom of the flat panel when the x-ray tube is stationed at its maximum vertical position. The resultant half fan angle is 11.9°.

2.A.4. Reconstruction

The reconstruction engine consists of a variation of the Feldkamp algorithm,[18] enabling it to run on a graphics processing unit (GPU). Each reconstruction is performed on a 4 GB GPU (GeForce GTX 690, NVIDIA, Santa Clara, CA) installed on a quad-core microprocessor computer with 32 GB memory.

Table I shows the system configurations of the previous and current generations of dedicated breast CT in our institution, along with the nicknames used for each scanner.

2.B. Detector modulation transfer function (MTF)

The detector MTF was measured at 60 kV with an edge phantom consisting of a 27 μm thick, 5×5 cm niobium filter supported by a 0.8 mm thick, 10×10 cm aluminum sheet.[19] The phantom was placed on the surface of the detector to eliminate the influence of the focal spot. In order to study the effects of cone-beam geometry on the detector MTF, the edge phantom was placed at two different positions on the detector plane: at the incident point of the central ray on detector and at the lower corner point. One hundred images were acquired at 60 kV, 160 mA, and 3 ms pulse width using an additional copper filtration of 0.25 mm and averaged to reduce random noise. Each experiment was repeated three times. In order to oversample the line spread function (LSF—similar to the Fujita or Judy method[20–22]), the phantom was placed at a slight angle with respect to the dexel grid of the detector (2°–4°). After detecting the edges using Otsu thresholding and Canny edge detection methods, the presampled MTF was computed using a synthesized oversampled LSF. All four edges of the phantom were extracted to generate corresponding LSFs. The final MTF was produced by averaging these measurements.

To analyze the effect of focal spot size on the system MTF, the edge phantom was positioned parallel to the plane of the detector panel at the isocenter with a small rotational angle, between 2° and 4°, to apply Fujita's method. Different binning modes were used in measuring the MTF to study the effects of different dexel sizes on the MTF. Comparative analysis was made using the two-sided paired t-test with statistical significance assumed at $P < 0.05$ in all cases.

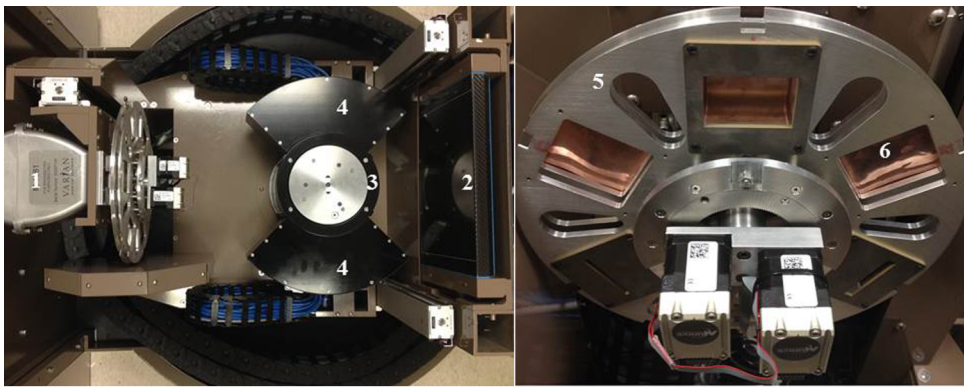

FIG. 2. Photographs of the gantry assembly designed for the latest UC Davis prototype of dedicated breast CT are pictured. The top view of the gantry and the filter/collimator changer assembly are shown in (a) and (b), respectively. The gantry components of the scanner are marked as follows: x-ray tube (1), flat-panel detector (2), central post (3), PET scanner heads (4), collimator changer (5), and filter changer (6).

TABLE I. System components and configurations used in generations of UC Davis dedicated breast CT.

Parameter	Albion and Bodega (1st generation)	Cambria (2nd generation)	Doheny (3rd generation)
X-ray tube	1 kW water-cooled, tungsten anode x-ray tube, running up to 12.5 mA at 80 kV	11.3 kW water-cooled, tungsten anode x-ray tube, running up to 240 mA at 60 kV	11.3 kW water-cooled, tungsten anode x-ray tube, running up to 240 mA at 60 kV
X-ray output	Continuous	Pulsed (pulse duty – cycle = 18%)	Pulsed (pulse duty-cycle = 9%–18%)
Nominal focal spot	0.4×0.4 mm	0.3×0.3 mm	0.3×0.3 mm
Additional filtration	0.30 mm of copper	0.25 mm of copper	0.10–0.35 mm of copper
Flat-panel detector	Varian Paxscan 4030CB	Varian Paxscan 4030CB	Dexela 2923 MAM
Magnification factor	1.92	1.90	1.39

2.C. System MTF

In order to generate the point spread function (PSF) using the reconstructed CT images, a 13 μm tungsten wire was placed at various positions in the detector's field of view. Eight hundred projections were acquired and used during the image reconstruction process. All the scans were performed at 60 kV, 180 mA, and a 3 ms pulse width. The tube potential selected was that previously calculated and reported to be the typical value used for patient breast scanning.[23] Projection images were acquired at the high-dose limit of the prototype scanner at 60 kV. As reported earlier,[24] due to the fact that only the wire was included during each scan, the MTFs stated here should be considered as the scatterfree MTF for this prototype breast CT system. It should be noted that the Nyquist frequency of the cone-beam CT scanner at isocenter was calculated as 9.3, 4.7, and 2.3 lp/mm for detector binning modes of 1×1, 2×2, and 4×4, respectively.[25]

A total of ten reconstructed slices were averaged to reduce noise. Due to the subtlety of the 13 μm wire, the location of the generated PSF was subject to minor planar translations. Accounting for the potential movement of the PSF, the following calculations were applied.

First, the center of mass along the x and y axes (CM_x and CM_y) for each PSF was computed as

$$CM_x = \sum_x \sum_y [ROI(x,y)\times x] \Big/ \sum_x \sum_y ROI(x,y) \quad (1a)$$

and

$$CM_y = \sum_x \sum_y [ROI(x,y)\times y] \Big/ \sum_x \sum_y ROI(x,y), \quad (1b)$$

where (x,y) is the spatial location of the pixel in the region of interest (ROI). Second, the calculated spatial coordinates of the PSF in the $x-y$ plane were translated to match the CM of the PSF on the adjacent layers.

Following the same experimental setup, a 70 μm nickel-chromium wire was used in separate experiments to study the effect of different wire diameters in generating point stimuli used in the system MTF calculations. Shown in Sec. 3.B, results validate the use of the 70 μm wire as a surrogate for the 13 μm tungsten wire. Therefore, the nickel-chromium wire was used for PSF generation during subsequent experiments.

To study the effects of the reconstruction filters on the MTF characteristics, other experiments were conducted. In accordance with our standard patient imaging protocol, 800 projection views were acquired at 2×2 high-gain binning mode at a rate of 50 frames per second (fps). Four types of reconstruction filters, Ramp, Shepp Logan, Cosine, and Hamming, were used.[19,26,27]

To study the effects of motion blurring on system MTF, the wire was placed at a radial distance of 71 mm away from the axes of rotation, accounting for an average breast diameter of 14 cm.[7] Two different numbers of projections, 800 and 500, were used.

2.D. System MTF comparison between different generations of bCT

For comparison of the spatial resolution characteristics of Doheny with the prior generations of bCT, Cambria and Bodega, similar setups were employed. In both cases, 500 images were acquired at 30 fps for a 16.6 s acquisition time; thus, Doheny's gantry motor rotational velocity is very similar to that of Bodega and Cambria. The Varian 4030CB detectors on both Cambria and Bodega were set to work in dynamic gain (unique to that detector system), with 2×2 binning mode. In each scanner, the 70 μm wire was used to generate the point stimuli, and wires were placed at the isocenter and periphery of the field of view. The same cone angle and reconstruction filter (Shepp-Logan) were used during the image reconstruction for all three bCT systems.

3. RESULTS

Figure 3 shows the distribution of the focal spot of the x-ray tube used in Cambria and Doheny over different mA values. Analyzing the images shown in Fig. 3(a), one can observe that the shape of the focal spot is comprised of a rectangle with two curvatures (or wings) on the left and right sides of the projected focal spot. The focal spot wings are caused by misfocused electrons originating from the cathode source. Line profiles of the focal spot at 60 kV and different corresponding mA values are shown in Fig. 3(b). Based on these results, it was concluded that the length and width of the projected focal spot at 60 kV were 0.49 and 0.34 mm, respectively.

The calculated detector MTF curves at 60 kV are shown in Fig. 4. Detector MTFs are shown in conjunction with the ideal MTF (calculated via the normalized sinc function utilizing detector element aperture size). Based on these results, the position of the edge phantom has a small effect on the detector MTF working at different binning modes. Comparing the

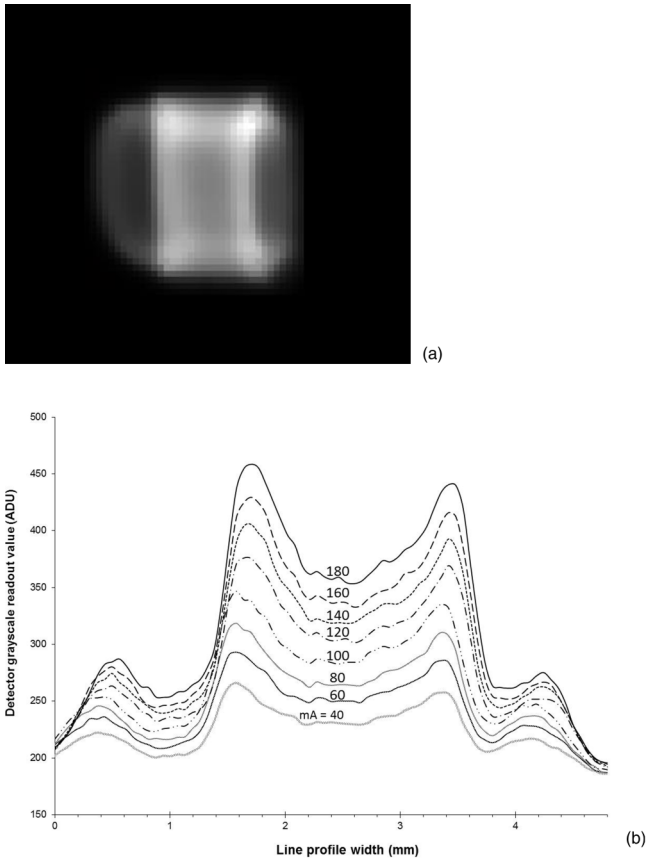

FIG. 3. (a) Focal spot of the x-ray tube used in Cambria and Doheny (M-1500, Varian Medical Systems, Salt Lake city, UT), (b) line profile representative of the distribution of the focal spot at 60 kV and different mA values along the horizontal axis passing through the projection of the focal spot on the detector.

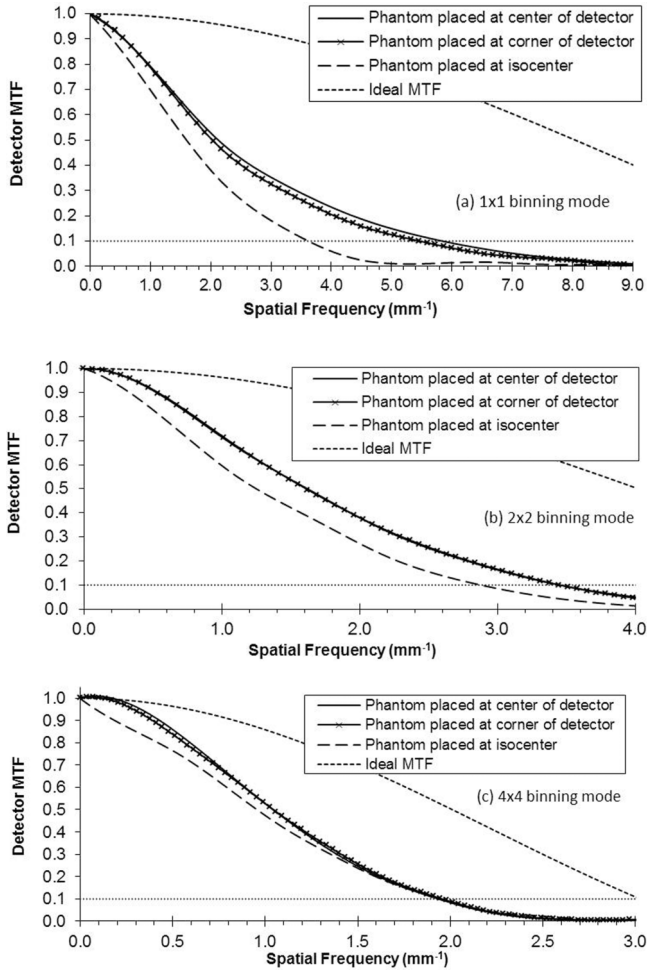

FIG. 4. Detector MTF (projection imaging) results measured for three different pixel binning modes. The edge phantom was placed at two different locations on the surface of the detector. In each binning mode, the edge phantom was imaged and averaged with 300 views at 60 kV, 160 mA, and 3 ms of pulse width. The detector was set to work at LFW mode with pixel binning set to 1×1 (a), 2×2 (b), and 4×4 (c).

two-sided paired t-test resulted in average values of 0.57, 0.67, and 0.75; therefore, over the frequencies between 0 and Nyquist for the binning modes of 1×1, 2×2, and 4×4, respectively, there was no statistical difference (i.e., $P >> 0.05$) between the "center" and "corner" detector MTF results. The detector MTFs at 10% max for 1×1, 2×2, and 4×4 binning modes were at 5.70, 3.45, and 1.95 line-pairs/mm. In addition, this figure shows the impact of the focal spot on the detector MTF. The maximum and minimum degradation in the detector MTF result when the detector is set to work in native and 4×4 binning modes, respectively.

Figure 5 demonstrates an alternative method of analyzing the detector MTF results. Referring to this figure, moving the edge phantom further away from the detector panel and closer to the x-ray tube, the observed reduction in the detector limiting resolution at 10% MTF was 35%, 14%, and 2% corresponding to the binning modes of 1×1, 2×2, and 4×4, respectively.

The effect of using the wires with different diameters on system MTF was studied in detector native binning mode. Results are shown in Fig. 6. For this experiment, the images were reconstructed at a cone angle of less than 1°. A two-sided paired t-test for the binning modes of 1×1, 2×2, and 4×4 resulted in average values of 0.54, 0.61, and 0.69, indicating no statistical difference; hence, it is reasonable to assume that the 70 μm nickel-chromium wire is essentially a point stimulus. This figure also shows the oversampling method used in generating PSFs. The CT images were reconstructed with two CT voxel sizes to emphasize the difference between the generated PSFs using 13 and 70 μm wires. Excessive oversampling at the reconstruction phase does not add more information concerning the MTF behavior of the system.

Figure 7 illustrates the impact of radial distance on the system MTF. The scans were performed at 60 kV and 432 mA s. Considering a detector frame rate of 50 fps, 16 s are required to acquire 800 images, which is the typical patient scan time used in our lab. The radial position was measured using the flat-fielded projection images. The wire was placed at a maximum distance of 71 mm from the axis of rotation of the scanner to assess the periphery of the average breast diameter. A cone angle of less than 1° was used during the scan and a Shepp-Logan filter was employed during the reconstruction. These results clearly validate the assumption that due to the relatively short pulse used in image acquisition, motion has minimal impact on the reconstructed CT image blurring.

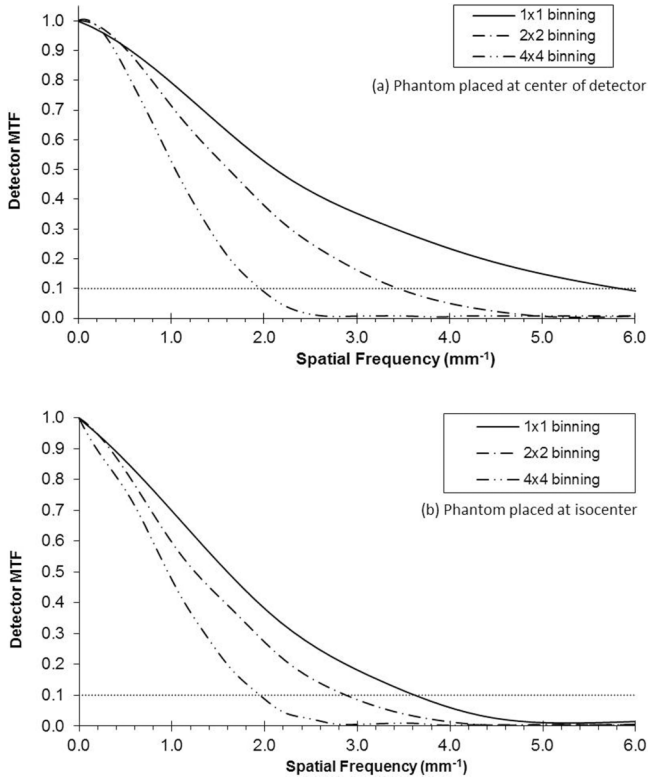

FIG. 5. Detector MTF results at different binning modes with edge phantom placed at (a) center of detector and (b) isocenter.

Figure 8 shows the impact of using different reconstruction filters. Here, the difference between the filters is the roll-off at higher frequencies. The roll-off effect results in a noise reduction, as well as a change in spatial resolution characteristics of the reconstructed images.

The results shown in Fig. 9 demonstrate the effect of using different number of views on the system MTF. Based on these results, one can observe that no significant improvement in MTF is achieved by increasing the number of views from 500 to 800. The experiment was performed at different detector binning modes. Throughout the experiments, the two-

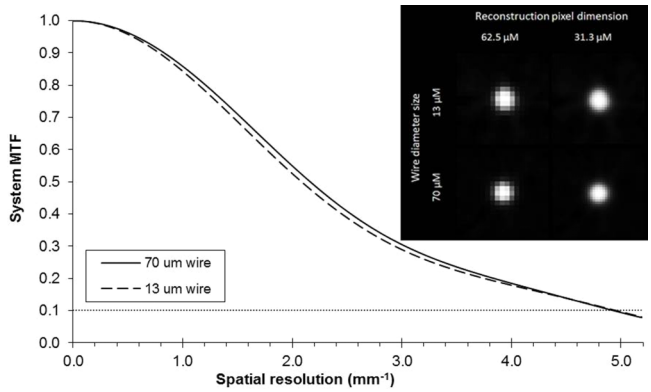

FIG. 6. The effect that the wire diameter has on the coronal plane MTF. The detector was set to work at high-gain 1×1 binning mode with a readout rate of 23.25 fps. The same technique factors and methods were used to measure the system MTF.

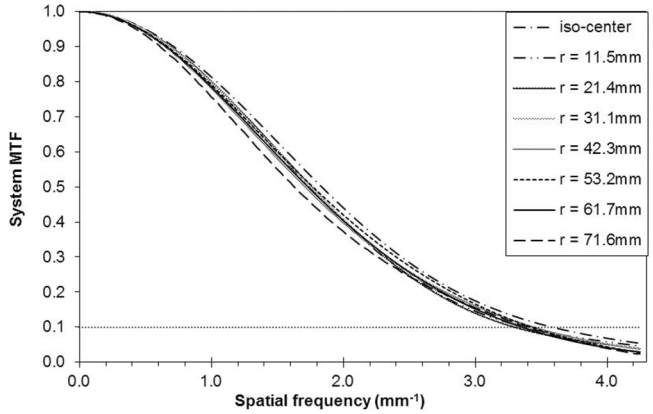

FIG. 7. The coronal plane MTF for eight different radial positions from the axis of rotation of the reconstructed image. A total of 800 projection images were acquired at a low full well, 2×2 binning mode, and a 50 fps frame rate. All images were reconstructed using the Shepp-Logan filter.

sided paired *t*-test results demonstrate no statistical difference between the system MTFs calculated with different number of views.

Figure 10 demonstrates a comparison between system MTFs when detector is set at different binning modes. Eight hundred views were acquired for each scan and the CT images were reconstructed using the Shepp-Logan filter.

Figure 11 shows a comparison between the spatial resolution characteristics of scanners Bodega, Cambria, and Doheny. Placing the wire at isocenter results in a minor improvement in system MTF between Bodega and Cambria, as shown in Fig. 11(a). This was expected given that both scanners use similar geometry and the same type of detector; however, a significant improvement in MTF is achieved in scanner Doheny due to the changes in geometry and use of a high resolution flat-panel detector. In addition, Fig. 11(b) demonstrates the impact of the gantry motion on the system MTF. The drop in the system MTF at higher frequencies in Bodega, a direct consequence of using a continuous x-

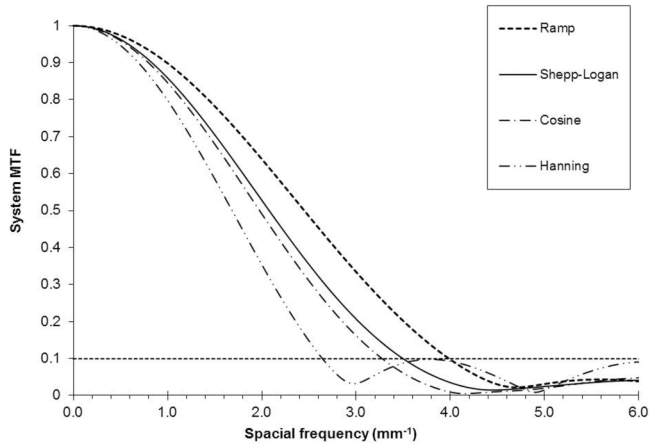

FIG. 8. The change in the MTF by switching to different reconstruction filters is shown. The detector was set to work at low full well, 2×2 binning mode with a 50 fps rate. Eight hundred views were used for the acquisition. CT images were reconstructed at a cone angle of less than 1°.

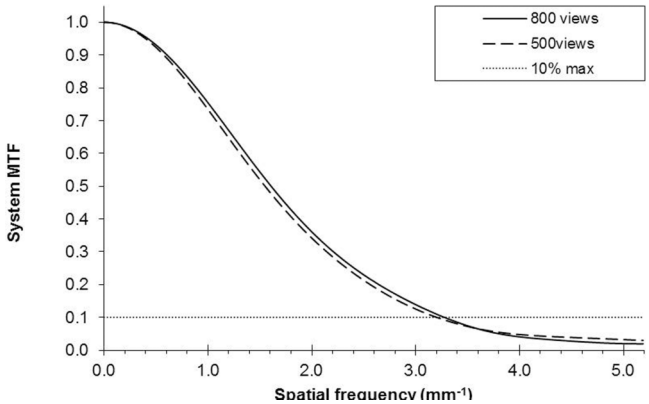

FIG. 9. System MTF characterization with different numbers of projection images. The detector was set to LFW, 2×2 binning mode with a frame rate of 50 fps. Scans were performed with identical x-ray technique factors.

ray source, was addressed in the design of the Cambria and Doheny scanners. In Bodega, the azimuthal MTF consistently drops from the isocenter to the periphery. Since the x-ray tube used in the later generations of CT is pulsed, x-rays are projected in only a fraction of each exposure period, resulting in restoration of the azimuthal MTF.

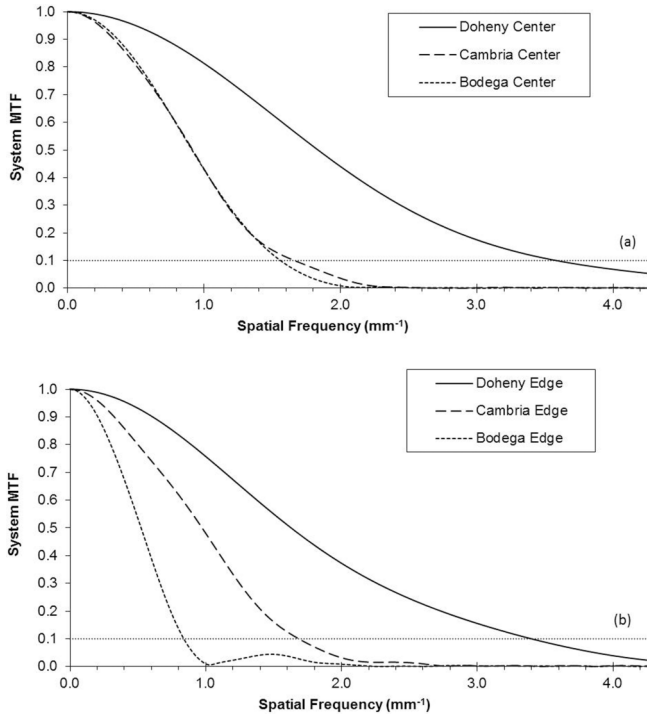

FIG. 11. A system MTF comparison between different generations of UC Davis dedicated breast CT is shown. The system MTF at the isocenter and the periphery of the FOV of each scanner is shown in (a) and (b), respectively.

4. DISCUSSION

Based on the results shown in Fig. 4, the oversampling method used in deriving the detector MTF is acceptable, as cone angle does not have a significant impact on the MTF. Results shown in this figure suggest that given correct flat-fielding of the raw projection images, the detector MTF is not affected by the location of the object in the detector field of view.

During a routine patient scan in our laboratory, the patient is instructed to hold their breath as 500–800 images are acquired over a period of 10–16 s. Using the detector in 1×1 binning mode requires a breath-hold period of up to 27 s—uncomfortable for most patients. Accounting for the flat-panel detector's frame rate, our laboratory's protocol, and efforts to minimize patient discomfort, 2×2 binning mode is currently being used during regular patient scans. Figure 5 shows that the further an object is moved from the detector, the greater the effect on MTF, especially for finer detector sampling (i.e., 1×1). This observation demonstrates the impact of focal spot size on the spatial resolution of this breast CT system.

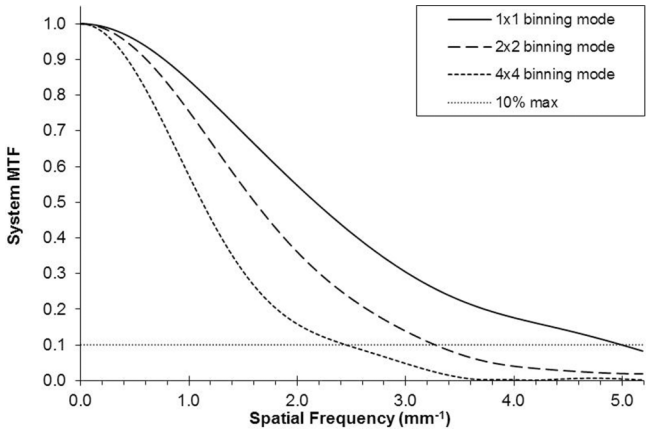

FIG. 10. A comparison between system MTFs with different detector binning modes is shown. Eight hundred images were acquired at LFW mode, with identical x-ray technique factors.

Results shown in Fig. 6 confirm that the 70 μm nickel-chromium wire is an adequate substitution for the 13 μm tungsten wire in generating the point stimulus required for measurement of the system MTF. Though these results justify the use of the 70 μm wire to facilitate experimentation, they also underscore the impact of focal spot size on spatial resolution in breast CT technology. Assuming that the focal spot is infinitesimally small, using a wire with a smaller diameter should result in better MTF, yet in Fig. 6, we showed that it does not. This highlights the focal spot size impact on the spatial resolution. As the Nyquist criterion has been met, reconstructing the CT images with smaller pixel sizes does not add new information. Moreover, the larger the reconstruction matrix, the longer the amount of time required for the reconstruction engine to produce the CT images and the greater the amount of disk space required to store them.

Figure 8 supports preservation of the image reconstruction protocol used in prior generations of bCT. Despite improvements in the system MTF, the ramp reconstruction filter exhibits poor noise characteristics and therefore would not be used in routine patient scans. Patient scan protocol in prior generations of bCT has suggested that the usage of the Shepp-

Logan filter is a reasonable kernel for image reconstruction. This filter maintains a good balance between noise and detail in the reconstructed image, supporting its continued usage.

By keeping the frame rate constant and using greater number of views reduces the gantry rotational speed, which had a large impact on the measured system MTF in Bodega. This is due to the limitation of designing a cone-beam CT system using a continuous x-ray source. Using the pulsed x-ray system in the second and third generations solved this problem. In Doheny, parameters resulting in a change of the gantry rotational speed have minimal impact on the system MTF. Figure 9 supports this observation and no observable degradation in the system MTF is seen in moving away from the center of rotation toward the periphery of the field of view.

Comparing the results shown in Figs. 4 and 10 provides an insight into the impact of system geometry, image reconstruction scheme, and the focal spot size on the spatial resolution. The magnification and the mathematical reconstruction filter lead to improvements in system MTF, while the focal spot size has a detrimental effect. The drop in the limiting resolution from 6.0 mm^{-1} (detector MTF) to 5.0 mm^{-1} (system MTF) at 1×1 binning mode highlights the effect of the focal spot size. At 2×2 binning mode, the drop of the limiting resolution decreases, proving that the magnification leads to a compensation of the modulation lost due to the focal spot size. The improvement in the limiting resolution from detector MTF to system MTF in the 4×4 binning mode indicates that larger dexel size decreases the effect of focal spot size on MTF, and in this case, magnification leads to an improvement in spatial resolution.

Figure 10 shows that a 30% improvement is possible when switching from 2×2 to 1×1 binning modes. The detector 1×1 binning mode with a maximum frame rate of 26 fps proves impractical for breath-hold imaging for 19.2 s. A gradual improvement is observed in the spatial resolution characteristics of the generations of UC Davis dedicated breast systems, as demonstrated in Fig. 10. Further studies of noise power spectrum (NPS) in conjunction with the MTF results presented in this study will clarify the optimal number of views and corresponding detector binning modes and technique factors for patient scans.

The focus of this research was on the spatial resolution in the coronal plane of the breast CT system, which is the inherent CT reconstruction plane for the dedicated breast imaging geometry of our systems. This study did not focus on resolution in the z-axis (A–P dimension), which affects the spatial resolution in the coronal and sagittal images on breast CT. Coronal images are not possible with digital mammography or tomosynthesis; sagittal breast CT images are similar in orientation to medial lateral oblique (MLO) images in digital mammography and tomosynthesis. Axial breast CT images are similar in orientation to the cranial caudal (CC) images in digital mammography and tomosynthesis. It should be noted that the z-axis of the breast CT images is not affected by the roll-off of the apodization filter used for CT reconstruction (e.g., Shepp-Logan filter). Therefore, the spatial resolution along the slice thickness domain in breast CT is essentially a RECT function, limited only by the slice thickness.

5. CONCLUSION

The four breast CT scanners that have been designed, fabricated, and tested at UC Davis have led to a number of reports in the literature, including both technical papers and results of several clinical trials. This communication is designed to describe, in detail, the evolution of spatial resolution in the breast CT scanners that have been designed and clinically tested at our facility. Our most recent scanner, Doheny, takes a big step forward with respect to spatial resolution, and this is due to the combination of a pulsed x-ray source, a smaller focal spot, and a higher resolution flat-panel detector. All of the previous reports which focus on patient imaging were produced on the first generation (Albion and Bodega) systems. As we begin clinical testing with the new higher spatial resolution breast CT scanner, with respect to microcalcification detection specifically, we hypothesize that comparisons between breast CT, digital mammography, and tomosynthesis will demonstrate more similar clinical performance than past comparisons.

ACKNOWLEDGMENTS

This work was supported in part by two research grants (Grant Nos. 7EB-0075 and 11I-0114) from California Breast Cancer Research Program, a research grant (Grant No. R01 CA89260) from National Cancer Institute, and a research grant (Grant No. R01 EB002138) from the National Institute of Biomedical Imaging and Bioengineering.

[a]Electronic mail: john.boone@ucdmc.ucdavis.edu

[1]A. T. Wang, J. Fan, H. K. Van Houten, J. C. Tilburt, N. K. Stout, V. M. Montori, and N. D. Shah, "Impact of the 2009 US Preventive Services Task Force guidelines on screening mammography rates on women in their 40s," PloS One **9**, e91399 (2014).

[2]D. H. Howard and E. K. Adams, "Mammography rates after the 2009 US Preventive Services Task Force breast cancer screening recommendation," Prev. Med. **55**, 485–487 (2012).

[3]M. T. Mandelson, N. Oestreicher, P. L. Porter, D. White, C. A. Finder, S. H. Taplin, and E. White, "Breast density as a predictor of mammographic detection: Comparison of interval- and screen-detected cancers," J. Natl. Cancer Inst. **92**, 1081–1087 (2000).

[4]D. Saslow, C. Boetes, W. Burke, S. Harms, M. O. Leach, C. D. Lehman, E. Morris, E. Pisano, M. Schnall, S. Sener, R. A. Smith, E. Warner, M. Yaffe, K. S. Andrews, and C. A. Russell, G. for the American Cancer Society Breast Cancer Advisory, "American Cancer Society guidelines for breast screening with MRI as an adjunct to mammography," Ca-Cancer J. Clin. **57**, 75–89 (2007).

[5]T. M. Kolb, J. Lichy, and J. H. Newhouse, "Comparison of the performance of screening mammography, physical examination, and breast US and evaluation of factors that influence them: An analysis of 27,825 patient evaluations," Radiology **225**, 165–175 (2002).

[6]W. A. Berg, J. D. Blume, J. B. Cormack, E. B. Mendelson, D. Lehrer, M. Bohm-Velez, E. D. Pisano, R. A. Jong, W. P. Evans, M. J. Morton, M. C. Mahoney, L. H. Larsen, R. G. Barr, D. M. Farria, H. S. Marques, and K. Boparai, "Combined screening with ultrasound and mammography vs mammography alone in women at elevated risk of breast cancer," JAMA, J. Am. Med. Assoc. **299**, 2151–2163 (2008).

[7]J. M. Park, E. A. Franken, Jr., M. Garg, L. L. Fajardo, and L. T. Niklason, "Breast tomosynthesis: Present considerations and future applications," Radiographics **27**(Suppl. 1), S231–S240 (2007).

[8]E. A. Rafferty, J. M. Park, L. E. Philpotts, S. P. Poplack, J. H. Sumkin, E. F. Halpern, and L. T. Niklason, "Diagnostic accuracy and recall rates for digital mammography and digital mammography combined with one-view

and two-view tomosynthesis: Results of an enriched reader study," AJR, Am. J. Roentgenol. **202**, 273–281 (2014).
[9]L. T. Niklason, B. T. Christian, L. E. Niklason, D. B. Kopans, D. E. Castleberry, B. H. Opsahl-Ong, C. E. Landberg, P. J. Slanetz, A. A. Giardino, R. Moore, D. Albagli, M. C. Dejule, P. F. Fitzgerald, D. F. Fobare, B. W. Giambattista, R. F. Kwasnick, J. Liu, S. J. Lubowski, G. E. Possin, J. F. Richotte, C. Y. Wei, and R. F. Wirth, "Digital tomosynthesis in breast imaging," Radiology **205**, 399–406 (1997).
[10]L. Chen, C. K. Abbey, A. Nosratieh, K. K. Lindfors, and J. M. Boone, "Anatomical complexity in breast parenchyma and its implications for optimal breast imaging strategies," Med. Phys. **39**, 1435–1441 (2012).
[11]P. Gazi, K. Yang, G. Burkett, and J. Boone, "Development and spatial resolution characterization of a dedicated pulsed x-ray, cone-beam breast CT system," Proc. SPIE **8668**, 86681D (2013).
[12]A. Kwan, N. Shah, G. Burkett, J. A. Seibert, K. K. Lindfors, T. R. Nelson, and J. M. Boone, "Progress in the development of a dedicated breast CT scanner," Proc. SPIE **5368**, 304–310 (2004).
[13]K. K. Lindfors, J. M. Boone, T. R. Nelson, K. Yang, A. L. Kwan, and D. F. Miller, "Dedicated breast CT: Initial clinical experience," Radiology **246**, 725–733 (2008).
[14]P. Gazi and J. M. Boone, "Improving the spatial resolution characteristics of dedicated cone-beam breast CT technology," Proc. SPIE **9033**, 903348 (2014).
[15]A. C. Konstantinidis, M. B. Szafraniec, L. Rigon, G. Tromba, D. Dreossi, N. Sodini, P. F. Liaparinos, S. Naday, S. Gunn, A. Mcarthur, R. D. Speller, and A. Olivo, "X-ray performance evaluation of the dexela CMOS APS x-ray detector using monochromatic synchrotron radiation in the mammographic energy range," IEEE Trans. Nucl. Sci. **60**, 3969–3980 (2013).
[16]S.-Y. Huang, J. M. Boone, K. Yang, N. J. Packard, S. E. Mckenney, N. D. Prionas, K. K. Lindfors, and M. J. Yaffe, " The characterization of breast anatomical metrics using dedicated breast CT," Med. Phys. **38**, 2180–2191 (2011).
[17]K. Yang, A. L. Kwan, D. F. Miller, and J. M. Boone, "A geometric calibration method for cone beam CT systems," Med. Phys. **33**, 1695–1706 (2006).
[18]L. A. Feldkamp, L. C. Davis, and J. W. Kress, "Practical cone-beam algorithm," J. Opt. Soc. Am. A **1**, 612–619 (1984).
[19]K. Yang, "Development and evaluation of a dedicated breast CT scanner," Ph.D. dissertation, University of California, Davis, 2007.
[20]H. Fujita, D. Y. Tsai, T. Itoh, K. Doi, J. Morishita, K. Ueda, and A. Ohtsuka, "A simple method for determining the modulation transfer function in digital radiography," IEEE Trans. Med. Imaging **11**, 34–39 (1992).
[21]P. F. Judy, "The line spread function and modulation transfer function of a computed tomographic scanner," Med. Phys. **3**, 233–236 (1976).
[22]E. Samei, M. J. Flynn, and D. A. Reimann, "A method for measuring the presampled MTF of digital radiographic systems using an edge test device," Med. Phys. **25**, 102–113 (1998).
[23]N. D. Prionas, S. Y. Huang, and J. M. Boone, "Experimentally determined spectral optimization for dedicated breast computed tomography," Med. Phys. **38**, 646–655 (2011).
[24]A. L. Kwan, J. M. Boone, K. Yang, and S. Y. Huang, "Evaluation of the spatial resolution characteristics of a cone-beam breast CT scanner," Med. Phys. **34**, 275–281 (2007).
[25]K. Yang, A. L. Kwan, S. Y. Huang, N. J. Packard, and J. M. Boone, "Noise power properties of a cone-beam CT system for breast cancer detection," Med. Phys. **35**, 5317–5327 (2008).
[26]J. T. Bushberg, *The Essential Physics of Medical Imaging*, 3rd ed. (Wolters Kluwer Health/Lippincott Williams & Wilkins, Philadelphia, 2012).
[27]A. C. Kak and M. Slaney, *Principles of Computerized Tomographic Imaging* (Society for Industrial and Applied Mathematics, Philadelphia, 2001).